Article

# A Proton-Shuttle Mechanism Mediated by the Porphyrin in Benzene Hydroxylation by Cytochrome P450 Enzymes

Sam P. de Visser, and Sason Shaik

*J. Am. Chem. Soc.*, **2003**, 125 (24), 7413-7424• DOI: 10.1021/ja034142f • Publication Date (Web): 22 May 2003



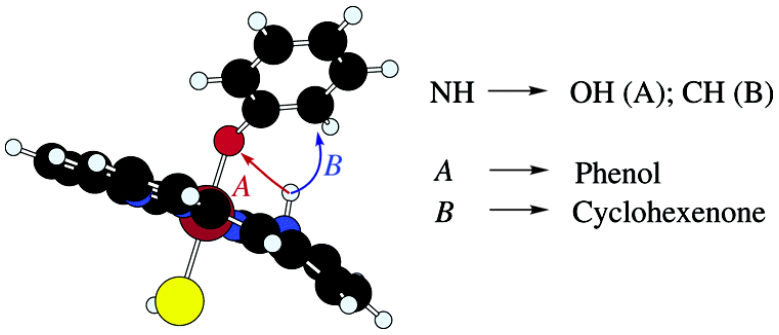


## More About This Article

Additional resources and features associated with this article are available within the HTML version:

- Supporting Information
- Links to the 23 articles that cite this article, as of the time of this article download
- Access to high resolution figures
- Links to articles and content related to this article
- Copyright permission to reproduce figures and/or text from this article

View the Full Text HTML

J|A|C|S
ARTICLES
Published on Web 05/22/2003

# A Proton-Shuttle Mechanism Mediated by the Porphyrin in Benzene Hydroxylation by Cytochrome P450 Enzymes

Sam P. de Visser and Sason Shaik*

*Contribution from the Department of Organic Chemistry and the Lise Meitner-Minerva Center for Computational Quantum Chemistry, The Hebrew University of Jerusalem, 91904 Jerusalem, Israel*

Received January 13, 2003; E-mail: sason@yfaat.ch.huji.ac.il

***Abstract:*** Benzene hydroxylation is a fundamental process in chemical catalysis. In nature, this reaction is catalyzed by the enzyme cytochrome P450 via oxygen transfer in a still debated mechanism of considerable complexity. The paper uses hybrid density functional calculations to elucidate the mechanisms by which benzene is converted to phenol, benzene oxide, and ketone, by the active species of the enzyme, the high-valent iron−oxo porphyrin species. The effects of the protein polarity and hydrogen-bonding donation to the active species are mimicked, as before (Ogliaro, F.; Cohen, S.; de Visser, S. P.; Shaik, S. *J. Am. Chem. Soc.* **2000**, *122*, 12892−12893). It is verified that the reaction does not proceed either by hydrogen abstraction or by initial electron transfer (Ortiz de Montellano, P. R. In *Cytochrome P450: Structure, Mechanism and Biochemistry*, 2nd ed.; Ortiz de Montellano, P. R., Ed.; Plenum Press: New York, 1995; Chapter 8, pp 245−303). In accord with the latest experimental conclusions, the theoretical calculations show that the reactivity is an interplay of electrophilic and radicalar pathways, which involve an initial attack on the $\pi$-system of the benzene to produce $\sigma$-complexes (Korzekwa, K. R.; Swinney, D. C.; Trager, W. T. *Biochemistry* **1989**, *28*, 9019−9027). The dominant reaction channel is electrophilic and proceeds via the cationic $\sigma$-complex, $^2$**3**, that involves an internal ion pair made from a cationic benzene moiety and an anionic iron porphyrin**.** The minor channel proceeds by intermediacy of the radical $\sigma$-complex, $^2$**2**, in which the benzene moiety is radicalar and the iron−porphyrin moiety is neutral. Ring closure in these intermediates produces the benzene oxide product ($^2$**4**), *which does not rearrange* to phenol ($^2$**7**) or cyclohexenone ($^2$**6**). While such a rearrangement can occur post-enzymatically under physiological conditions by acid catalysis, the computations reveal a novel mechanism whereby the active species of the enzyme catalyzes directly the production of phenol and cyclohexenone. *This enzymatic mechanism involves proton shuttles mediated by the porphyrin ring through the N-protonated intermediate*, $^2$**5**, which relays the proton either to the oxygen atom to form phenol ($^2$**7**) or to the *ortho*-carbon atom to produce cyclohexenone product ($^2$**6**). The formation of the phenol via this proton-shuttle mechanism will be competitive with the nonenzymatic conversion of benzene oxide to phenol by external acid catalysis. With the assumption that $^2$**5** is not fully thermalized, this novel mechanism would account also for the observation that there is a partial skeletal retention of the original hydrogen of the activated C−H bond, due to migration of the hydrogen from the site of hydroxylation to the adjacent carbon (so-called "NIH shift" (Jerina, D. M.; Daly, J. W. *Science* **1974**, *185*, 573−582)). *Thus, in general, the computationally discovered mechanism of a porphyrin proton shuttle suggests that there is an enzymatic pathway that converts benzene directly to a phenol and ketone, in addition to nonenzymatic production of these species by conversion of arene oxide to phenol and ketone*. The potential generality of protonated porphyrin intermediates in P450 chemistry is discussed in the light of the H/D exchange observed during some olefin epoxidation reactions (Groves, J. T.; Avaria-Neisser, G. E.; Fish, K. M.; Imachi, M.; Kuczkowski, R. *J. Am. Chem. Soc.* **1986**, *108*, 3837−3838) and the general observation of heme alkylation products (Kunze, K. L.; Mangold, B. L. K.; Wheeler, C.; Beilan, H. S.; Ortiz de Montellano, P. R. *J. Biol. Chem.* **1983**, *258*, 4202−4207). The competition, similarities, and differences between benzene oxidation viz. olefin epoxidation and alkanyl C−H hydroxylation are discussed, and comparison is made with relevant experimental and computational data. The dominance of low-spin reactivity in benzene hydroxylation viz. two-state reactivity (Shaik, S.; de Visser, S. P.; Ogliaro, F.; Schwarz, H.; Schröder, D. *Curr. Opin. Chem. Biol.* **2002**, *6*, 556−567) in olefin epoxidation and alkane hydroxylation is traced to the loss of benzene resonance energy during the bond activation step.

## Introduction

Arene hydroxylation by the enzyme cytochrome P450 still poses tantalizing questions, concerning both the reaction mechanism and the toxicity of some of the metabolites.[1,2] The reaction produces typically three types of products, phenol, cyclohexenone, and arene oxide, which are shown below in the

***Scheme 1.*** Experimentally Based Alternative Mechanistic Hypotheses for the Hydroxylation of Benzene by Compound I (Cpd I)[a]

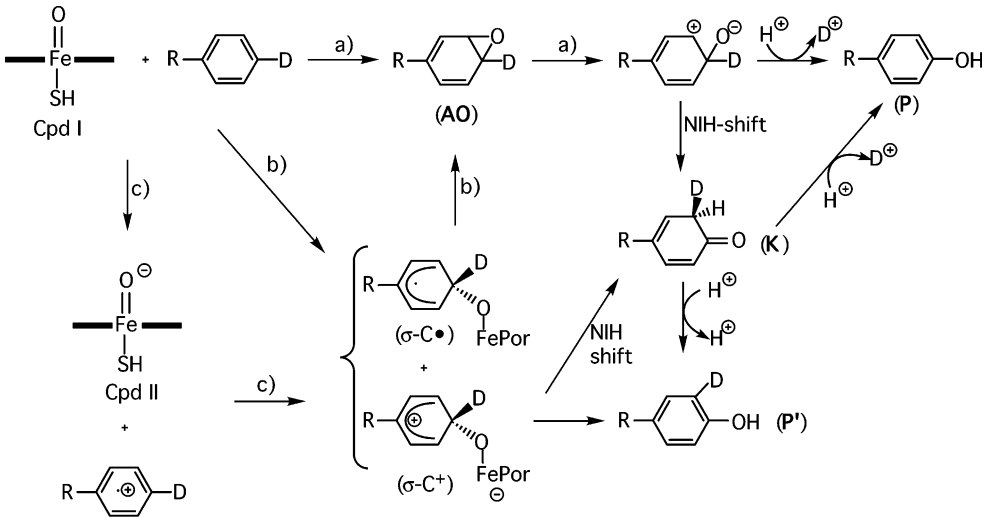


[a] In mechanism (a), arene oxide (AO) is the precursor of all other products. In mechanism (b), AO is formed from the radical $\sigma$-complex ($\sigma$-C•), while the ketone (K) and phenol (P, P′) are formed from the cationic $\sigma$-complex ($\sigma$-$C^+$).

reaction for benzene as an example.

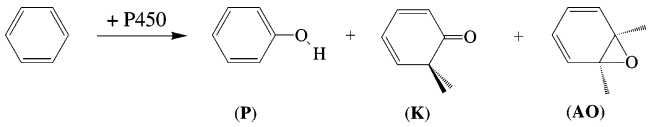


The P450 mediated conversion of arene to phenol (**P**) has traditionally been viewed as a means of detoxification and excretion of the toxic arene by the biosystem. By contrast, arene oxide (**AO**) is carcinogenic and mutagenetic through its interaction with, for example, DNA and other cellular material,[3,4] and is hence detrimental to the biosystem. The relationship between the two products became intriguing when mechanistic investigations[4] led to the conclusion that the highly toxic arene oxide is an intermediate in this reaction and the phenol is one of its byproducts. Further studies have led to the conclusion[5] that arene oxide is an obligatory intermediate in arene hydroxylation. However, in the course of time, new evidence has appeared that questioned the obligatory intermediacy of the arene oxide, thus proposing alternative pathways.[1,2,6,7] However, based on the detailed analysis of Ortiz de Montellano,[1] it is fair to say that as yet there is no consensus mechanism that is unequivocally established or that can rule out all others. Scheme 1 summarizes the main mechanistic hypotheses for arene hydroxylation by Compound I (Cpd I), the active species of the enzyme.[1,2]

A universal feature of arene hydroxylation[1,2,4] is the migration of the substituent from the site of hydroxylation to the adjacent carbon (so-called "NIH shift"). The substituent migration results in a partial skeletal retention of the original hydrogen of the activated C−H bond. This observation, which is inconsistent with the standard rebound mechanism[8] that operates in alkane hydroxylation, leaves in Scheme 1 those hypotheses that account for the NIH shift. For clarity, we labeled in the scheme the migrating hydrogen atom with D to identify the position of this atom in all intermediates.[2] In mechanism (a),[4a] everything is channeled through the arene oxide (**AO**), which is the primary product of the enzymatic reaction. In a subsequent *nonenzymatic step*, the epoxide ring opens to the zwitterionic species, which can further react in two different manners: a hydrogen/deuterium exchange will produce phenol (**P**, **P′**), whereas a 1,2-hydride (deuteride) shift to the carbocationic center (NIH shift) will give rise to cyclohexenone (**K**) that can, in turn, enolize to the phenol.[1,2,4] Mounting experimental evidence, of various kinds, has revealed, however, that phenol and ketone are unlikely to proceed through arene oxide.[6,7] Hence, in the alternative mechanistic hypothesis (b), all products are generated from the tetrahedral intermediate $\sigma$-complexes; the phenol and ketone are generated directly from the intermediate cationic $\sigma$-complex ($\sigma$-$\mathbf{C}^+$), Scheme 1,[6,7,9] while arene oxide formation is suggested[7] to transpire from the radical $\sigma$-complex intermediate ($\sigma$-**C**•). Details and pieces of mechanism (b) have gained indirect support from kinetic isotope effect measurements,[6] regiochemical studies,[7] frontier orbital theoretic arguments, and local density $X\alpha$ type calculations that ruled out concerted epoxidation as the initial activation step of substituted benzene by Cpd I.[10] A related mechanism (c)[1,2,11−13] that involves an initial electron transfer, followed by collapse to the $\sigma$-complexes, was suggested

(1) Ortiz de Montellano, P. R. In *Cytochrome P450: Structure, Mechanism and Biochemistry*, 2nd ed.; Ortiz de Montellano, P. R., Ed. Plenum Press: New York, 1995; Chapter 8, pp 245−303.
(2) Sono, M.; Roach, M. P.; Coulter, E. D.; Dawson, J. H. *Chem. Rev.* **1996**, *96*, 2841−2887.
(3) (a) Boyland, E. *Biochem. Soc. Symp.* **1950**, *5*, 40. (b) Boyland, E.; Sims, P. *Biochem. J.* **1965**, *95*, 788−792.
(4) (a) Jerina, D. M.; Daly, J. W. *Science* **1974**, *185*, 573−582. (b) Jerina, D. M.; Daly, J. W.; Witkop, B.; Zaltzman-Nirenberg, P.; Udenfriend, S. *Arch. Biochem. Biophys.* **1968**, *128*, 176−183.
(5) (a) Jerina, D. M.; Daly, J. W.; Witkop, B.; Zaltzman-Nirenberg, P.; Udenfriend, S. *J. Am. Chem. Soc.* **1968**, *90*, 6525−6527. (b) Jerina, D. M.; Daly, J. W.; Witkop, B.; Zaltzman-Nirenberg, P.; Udenfriend, S. *Biochemistry* **1970**, *9*, 147−156.
(6) Korzekwa, K. R.; Swinney, D. C.; Trager, W. T. *Biochemistry* **1989**, *28*, 9019−9027.
(7) Rietjens, I. M. C. M.; Soffers, A. E. M. F.; Veeger, C.; Vervoort, J. *Biochemistry* **1993**, *32*, 4801−4812.
(8) Groves, J. T.; McClusky, G. A. *J. Am. Chem. Soc.* **1976**, *98*, 859−861.
(9) Hanzlik, R. P.; Hogberg, K.; Judson, C. M. *Biochemistry* **1984**, *23*, 3048−3055.
(10) (a) Zakharieva, O.; Grodzicki, M.; Trautwein, A. X.; Veeger, C.; Rietjens, I. M. C. M. *J. Biol. Inorg. Chem.* **1996**, *1*, 192−204. (b) Zakharieva, O.; Grodzicki, M.; Trautwein, A. X.; Veeger, C.; Rietjens, I. M. C. M. *Biophys. Chem.* **1998**, *73*, 189−203.
(11) Guengerich, F. P.; MacDonald, T. L. *FASEB J.* **1990**, *4*, 2453−2459.
(12) Cavalieri, E. L.; Rogan, E. G. *Pharmac. Ther.* **1992**, *55*, 183−199.
(13) Burka, L. T.; Plucinski, T. M.; MacDonald, T. L. *Proc. Natl. Acad. Sci. U.S.A.* **1983**, *80*, 6680−6684.

too, but the existence of a free (diffusive) radical cation of the arene has not been demonstrated yet.[1,2,6,14] The role of charge transfer from the arene to the iron porphyrin has nevertheless been inferred from the kinetic isotope effect, for example, for the *meta* hydroxylation of chlorobenzene.[6]

Clearly, the catalysis of arene hydroxylation by P450 offers a rich and complex mechanistic puzzle. Despite the support accumulated thus far for the $\sigma$-complex based mechanism (b), there still exist counter arguments and compelling evidence for the intermediacy of benzene oxide, as in mechanism (a).[1,4] Furthermore, the postulated pathways that lead to arene oxide vis-à-vis phenol/ketone products are still under debate. Is the arene oxide intermediary tenable? Are there really both radicalar and carbocationic $\sigma$-complexes?[6] And if they exist, how precisely do they rearrange to yield ketone and phenol products? Since some cases of arene hydroxylation proceed by the complete loss of the original hydrogen in the C−H bond[1,9,15] and others by hydrogen abstraction from N−H[1,16] and O−H[1,17] bonds, for example, in phenacetin,[1] one may wonder whether the usual rebound mechanism is not, after all, competitive with (a)−(c)? And finally, Guengerich and MacDonald[11] proposed a unified scheme for arene hydroxylation and olefin epoxidation, which involves an interplay of mechanisms similar to those in Scheme 1. Since such unification is important, it is essential to outline the similarities and differences of arene hydroxylation and olefin epoxidation.[18−20]

Quantum mechanical calculations can probe subtle mechanistic questions of this type and complement thereby experimental information. Accordingly, the present paper uses hybrid density functional theoretical (DFT) calculations to address these mechanistic issues and compare them with previously studied mechanisms of alkene epoxidation and alkane hydroxylation.[21−25] It will be shown that, by contrast to other processes, which proceed by two-state reactivity involving both quartet and doublet spin states,[21,22,25] benzene hydroxylation is fundamentally different and is dominated by a single spin state, due to a unique feature of arene activation—the loss of resonance energy in the transition state. The calculations will also reveal a key role played by the porphyrin ligand. Thus, porphyrin acts as the springboard that mediates a proton shuttle, to-and-fro, and thereby provides *a channel that bypasses the arene oxide and directly converts the cationic σ-complex intermediates to phenol and ketone*. This novel feature resolves much of the mechanistic puzzle and makes a fruitful connection to other features of P450 reactivity, such as the heme alkylation side reaction that destroys the enzyme during its process of olefin epoxidation[26] and intriguing findings of hydrogen/deuterium exchange, reported for propene epoxidation[27] and a few other simple olefins, and so on.

## Methods

The DFT calculations employed the unrestricted UB3LYP method[28,29] in combination with an LACVP basis set[30] on iron and a 6-31G basis set on all other atoms. Geometries were optimized with JAGUAR 4.1,[31] while frequency analyses were done with GAUSSIAN98.[32] Transition states were verified by their appropriate single imaginary frequency. Reaction paths were explored by running stepwise geometry optimizations with an appropriate degree of freedom as a reaction coordinate. For space economy, these scans are presented in the Supporting Information deposited with this paper. Based on previous work,[22,25] we used Cpd I[33,34] with porphine to represent the native porphyrin ligand and $SH^-$ to represent the cysteinate ligand. Recent QM/MM studies in collaboration with the Mülheim group showed that this type of model represents the active site of P450 quite well.[35]

Electronic structures were ascertained by transforming the UKS orbitals of UB3LYP to natural orbitals, which are more amenable to electronic structure analysis.[36,37] Electronic effects of the protein environment were mimicked, as before,[22,33a] using two ammonia molecules that maintain NH···S hydrogen bonds to the thiolate ligand ($r_{NS}$ = 2.660 Å) and a polarizing environment with a dielectric constant $\epsilon$ equal to 5.7. These simple means represent reasonably well the polarity and hydrogen bonding capability of the protein pocket as revealed by the recent QM/MM calculations.[35]

## Results

Our study consists of testing and comparing four alternative mechanistic schemes for benzene hydroxylation, mechanisms (a)−(c) in Scheme 1 and, in addition, the usual rebound mechanism for alkane hydroxylation.[8] The study generated a great deal of data, which are summarized in the Supporting Information deposited with this paper, while the following discussion focuses on the lowest energy pathways and key features.


(14) (a) Riley, P.; Hanzlik, R. P. *Xenobiotica* **1994**, *24*, 1−16. (b) Hanzlik, R. P.; King, K.-H. J. *J. Am. Chem. Soc.* **1993**, *115*, 9363−9370.
(15) (a) Tomaszewski, J. E.; Jerina, D. M.; Daly, J. W. *Biochemistry* **1975**, *14*, 2024−2031. (b) Preston, B. D.; Miller, J. A.; Miller, E. C. *J. Biol. Chem.* **1983**, *258*, 8304−8311.
(16) (a) Hinson, J. A.; Nelson, S. D.; Mitchell, J. R. *Mol. Pharmacol.* **1977**, *13*, 625−633. (b) Hinson, J. A.; Nelson, S. D.; Gillette, J. R. *Mol. Pharmacol.* **1979**, *15*, 419−427. (c) Koymans, L.; van Lenthe, J. H.; Donné-Op den Kelder, G. M.; Vermeulen, N. P. E. *Mol. Pharmacol.* **1990**, *37*, 452−460.
(17) Ohe, T.; Mashnoa, T.; Hirobe, M. *Arch. Biochem. Biophys*. **1994**, *310*, 402−409.
(18) Groves, J. T.; Hang, Y.-Z. In *Cytochrome P450: Structure, Mechanism and Biochemistry*, 2nd ed.; Ortiz de Montellano, P. R., Ed. Plenum Press: New York, 1995; Chapter 1, pp 3−48.
(19) Woggon, W.-D. *Top. Curr. Chem.* **1996**, *184*, 40−96.
(20) Gross, Z.; Nimri, S.; Barzilay, C. M.; Simkhovich, L. *J. Biol. Inorg. Chem.* **1997**, *2*, 492.
(21) (a) de Visser, S. P.; Ogliaro, F.; Harris, N.; Shaik, S. *J. Am. Chem. Soc.* **2001**, *123*, 3037−3047. (b) de Visser, S. P.; Ogliaro, F.; Shaik, S. *Chem. Commun.* **2001**, 2322−2323. (c) de Visser, S. P.; Ogliaro, F.; Shaik, S. *Angew. Chem., Int. Ed.* **2001**, *40*, 2871−2874.
(22) (a) de Visser, S. P.; Ogliaro, F.; Sharma, P. K.; Shaik, S. *J. Am. Chem. Soc.* **2002**, *124*, 11809−11826. (b) de Visser, S. P.; Ogliaro, F.; Sharma, P. K.; Shaik, S. *Angew. Chem., Int. Ed.* **2002**, *41*, 1947−1951.
(23) (a) Yoshizawa, K.; Kagawa, Y.; Shiota, Y. *J. Phys. Chem. B* **2000**, *104*, 12365−12370. (b) Yoshizawa, K.; Kamachi, T.; Shiota, Y. *J. Am. Chem. Soc.* **2001**, *123*, 9806−9816. (c) Yoshizawa, K. *Coord. Chem. Rev.* **2002**, *226*, 251−259.
(24) Harris, D. L.; Loew, G. H. *J. Am. Chem. Soc.* **1995**, *117*, 2738−2746.
(25) (a) Ogliaro, F.; Harris, N.; Cohen, S.; Filatov, M.; de Visser, S. P.; Shaik, S. *J. Am. Chem. Soc.* **2000**, *122*, 8977−8989. (b) Ogliaro, F.; Filatov, M.; Shaik, S. *Eur. J. Inorg. Chem.* **2000**, 2455−2458.
(26) (a) Ortiz de Montellano, P. R.; Beilan, H. S.; Kunze, K. L.; Mico, B. A. *J. Biol. Chem.* **1981**, *256*, 4395−4399. (b) Kunze, K. L.; Mangold, B. L. K.; Wheeler, C.; Beilan, H. S.; Ortiz de Montellano, P. R. *J. Biol. Chem.* **1983**, *258*, 4202−4207. (c) Ortiz de Montellano, P. R.; Mangold, B. L. K.; Wheeler, C.; Kunze, K. L.; Reich, N. O. *J. Biol. Chem.* **1983**, *258*, 4208−4213. (d) Ortiz de Montellano, P. R. *Acc. Chem. Res.* **1987**, *20*, 289−294. (e) Mashiko, T.; Dolphin, D.; Nakano, T.; Traylor, T. G. *J. Am. Chem. Soc.* **1985**, *107*, 3735−3736. (f) Dexter, A. F.; Hager, L. P. *J. Am. Chem. Soc.* **1995**, *117*, 817−818. (g) Debrunner, P. G.; Dexter, A. F.; Schulz, C. E.; Xia, Y.-M.; Hager, L. P. *Proc. Natl. Acad. Sci. U.S.A.* **1996**, *93*, 12791−12798.
(27) Groves, J. T.; Avaria-Neisser, G. E.; Fish, K. M.; Imachi, M.; Kuczkowski, R. L. *J. Am. Chem. Soc.* **1986**, *108*, 3837−3838.
(28) Becke, A. D. *J. Chem. Phys.* **1992**, *96*, 2155−2160; ibid. **1992**, *97*, 9173−9177; ibid. **1993**, *98*, 5648−5652.
(29) Lee, C.; Yang, W.; Parr, R. G. *Phys. Rev. B* **1988**, *37*, 785−789.
(30) Hay, J. P.; Wadt, W. R. *J. Chem. Phys.* **1985**, *82*, 299−310.
(31) *Jaguar 4.1*; Schrödinger, Inc.: Portland, OR, 1998.
(32) *Gaussian-98*; Pittsburgh, PA, 1998.
(33) (a) Ogliaro, F.; Cohen, S.; de Visser, S. P.; Shaik, S. *J. Am. Chem. Soc.* **2000**, *122*, 12892−12893. (b) Ogliaro, F.; de Visser, S. P.; Cohen, S.; Kaneti, J.; Shaik, S. *ChemBioChem.* **2001**, *2*, 848−851.
(34) Harris, D. L. *Curr. Opin. Chem. Biol.* **2001**, *5*, 724−735.
(35) Schöneboom, J. C.; Reuter, N.; Lin, H.; Thiel, W.; Cohen, S.; Ogliaro, F.; Shaik, S. *J. Am. Chem. Soc.* **2002**, *124*, 8142−8151.
(36) Green, M. T. *J. Am. Chem. Soc.* **1998**, *120*, 10772−10773.
(37) Green, M. T. *J. Am. Chem. Soc.* **1999**, *121*, 7939−7940.

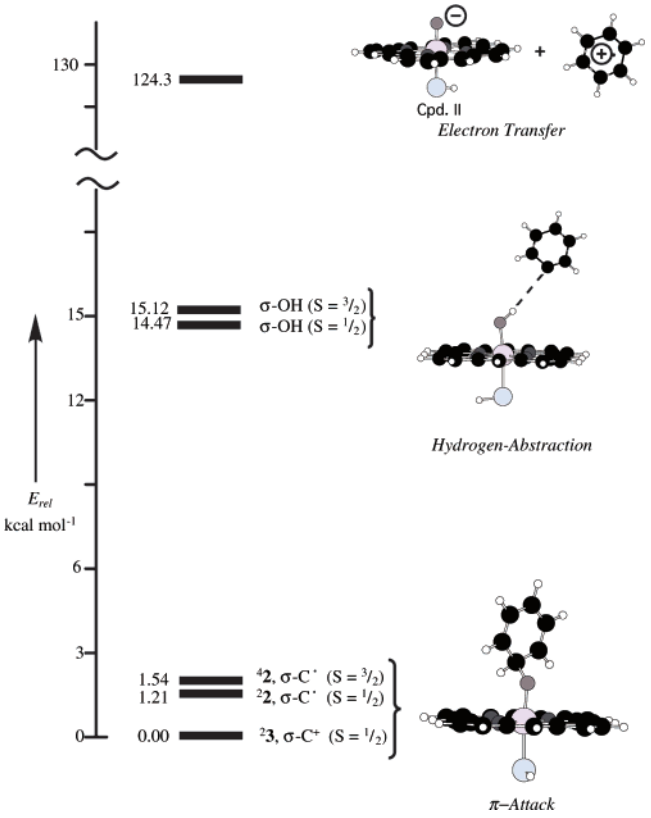


***Figure 1.*** Computed relative energies (in kcal mol$^{-1}$) of reaction intermediates for the mechanistic alternatives (a) and (c) in Scheme 1 and for the rebound mechanism. Relative energy and spin quantum number ($S$) are indicated in parentheses near each species. $^2$**2** and $^2$**3** are the corresponding radical and cationic $\sigma$-complexes of mechanism (b). The $\sigma$-OH is the species obtained by hydrogen abstraction from benzene in the rebound mechanism. The uppermost species correspond to the electron-transfer process in mechanism (c).

**A. Selection of the Lowest Energy Mechanisms.** Figure 1 shows the relative energy of the intermediates in the various mechanisms. All in all, we located 14 different intermediate structures nascent from the mechanisms in Scheme 1 and the rebound mechanism. The relative energies of these intermediates were calculated in vacuum and with the inclusion of the environmental effects. These data are summarized in the Supporting Information, while Figure 1 shows only the lowest states of each variety. It is seen that the lowest energy intermediates involve $\pi$-attack to generate the radicalar and carbocationic $\sigma$-complexes. The lowest intermediate is the carbocationic $\sigma$-complex, which has a doublet spin ($S = {}^1/_2$), and just slightly above it, there are two radicalar $\sigma$-complexes, in two spin varieties doublet and quartet ($S = {}^3/_2$). The quartet carbocationic $\sigma$-complex is much higher lying at 10.95 kcal mol$^{-1}$ and not shown in the figure. Still higher, at ca. 14−15 kcal mol$^{-1}$, are the lowest intermediates that are obtained by hydrogen abstraction, $\sigma$-OH. And finally, the electron transferred species lie more than 100 kcal mol$^{-1}$ above the lowest intermediates. Since the barriers to the formation of these intermediates are at least as high as the intermediates themselves, this rules out the electron transfer and the rebound mechanisms as viable alternatives for benzene hydroxylation. Indeed, the complete rebound mechanism was followed, and its barriers are at least 10 kcal mol$^{-1}$ higher than those for the formation of the radicalar and carbocationic $\sigma$-complexes (the hydrogen abstraction profile is given in the Supporting Information, Figure S.10). The results for the ET mechanism show that a diffusive arene radical cation will be hard to realize[1] even for arenes that are better electron donors than benzene. Therefore, we focus hereafter on the mechanisms that involve $\pi$-attack, (a) and (b) in Scheme 1.

**B. Mechanism of Benzene Epoxidation.** Step 1 of mechanism (a) involves a concerted epoxidation of benzene. $X\alpha$ type calculations by Zakharieva et al.[10] rule out the concerted arene oxide mechanism. In a recent study,[21b] we showed that a concerted epoxidation of ethene is a high energy process, and its transition structure is a second-order saddle point, with two negative frequencies. One corresponding to the oxygen insertion and the other connects the transition structure to the lower lying nonsynchronous transition state for epoxidation; in this case, this would be the transition state(s) for mechanism (b). It was shown that this is a general feature of the oxygen insertion that behaves like a forbidden reaction.[21b,38] Based on all these data, we can rule out the concerted epoxidation of benzene. Therefore, we are only left with mechanism (b) that proceeds via the radicalar and carbocationic $\sigma$-complexes and is the lowest energy pathway that has to account for the formation of benzene oxide, phenol, and ketone products.

**B.1. Radical and Electrophilic Reaction Profiles for Benzene Epoxidation.** Figure 2 summarizes the essential features of the three lowest energy pathways for benzene epoxidation starting with benzene and Cpd I ($^{4,2}$**1**) leading to benzene oxide ($^{4,2}$**4**). Both mechanisms proceed via an initial formation of a $\sigma$-complex ($^{4,2}$**2** and $^2$**3**), followed by ring closures to the arene oxide. One mechanism involves a radical-type attack, via $^{4,2}$**TS**$_{1,2}$, and results in the radical $\sigma$-complexes, $^{4,2}$**2**. By contrast, the second mechanism involves an electrophilic attack on benzene, via $^2$**TS**$_{1,3}$, and generates the carbocationic $\sigma$-complex, $^2$**3**. The lowest barrier in the gas phase is via $^2$**TS**$_{1,2}$ and is 17.5 kcal mol$^{-1}$ above the energy of the separate reactants, with the barrier via $^2$**TS**$_{1,3}$ only 0.6 kcal mol$^{-1}$ higher. All these intermediates undergo ring closure to the benzene oxide with small to moderate barriers.

**B.2. Bond Activation Transition States and Barriers.** The $^{4,2}$**TS**$_{1,2}$ species shown in Figure 2 are the quartet and doublet transition states (TSs) for the radicalar mechanism. It is seen that the low-spin species, $^2$**TS**$_{1,2}$, is significantly lower than the high-spin one, $^4$**TS**$_{1,2}$, unlike the situation in alkene epoxidation where the two species have similar energies.[21,22] Compared with the doublet species, $^4$**TS**$_{1,2}$ is more advanced (e.g., shorter O···C bond) with a higher degree of benzene activation (see later). As discussed later, this is the root cause of the clear separation of the spin state profiles for benzene activation as opposed to their proximity for olefin activation. The third TS species in Figure 2 is the doublet $^2$**TS**$_{1,3}$ that leads to the carbocationic $\sigma$-complex, $^2$**3**. The corresponding high-spin species, $^4$**TS**$_{1,3}$, is much higher lying (by 11.1 kcal mol$^{-1}$; see Supporting Information) and is therefore not shown here.

An indication of the different nature of the two mechanisms, radicalar viz. cationic, can be gained from the data in Table 1. The data shows different sensitivities of $^{4,2}$**TS**$_{1,2}$ viz. $^2$**TS**$_{1,3}$ to environmental effects, which were estimated from single point calculations with either two NH···S hydrogen bonds or a polarizing environment with a dielectric constant, $\epsilon$, of 5.7, or the combined effects. Thus, in a polarizing environment with a

(38) Sevin, A.; Fontecave M. *J. Am. Chem. Soc.* **1986**, *108*, 3266−3272.

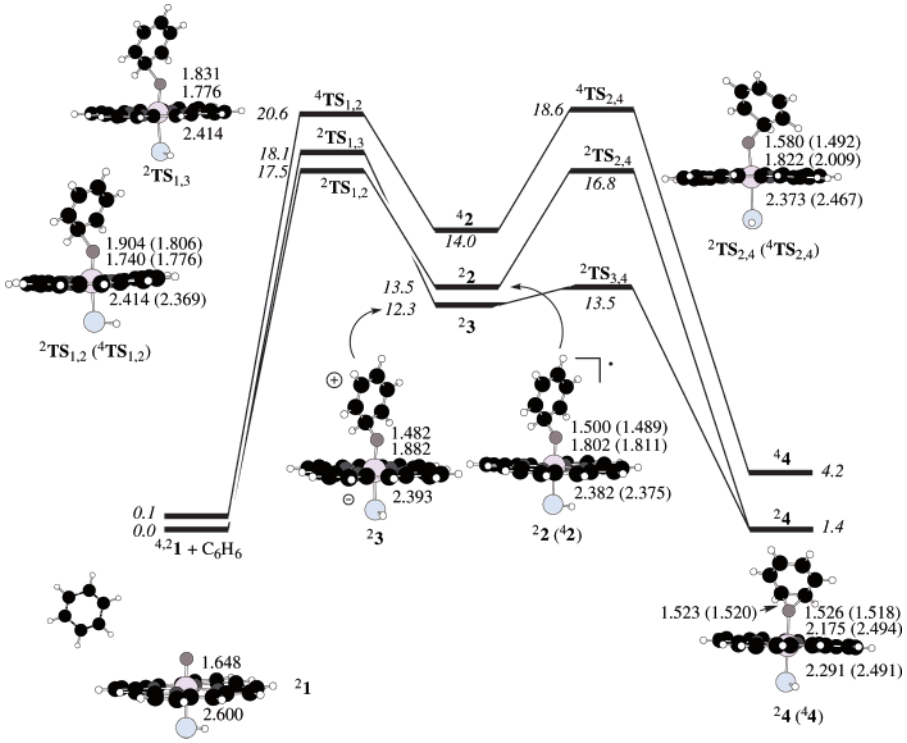


***Figure 2.*** Lowest doublet and quartet spin potential energy profiles for the formation of benzene oxide. All values are in kcal mol$^{-1}$ relative to the reactants. The $\sigma$-complexes $^{4,2}$**2** and $^2$**3** are radicalar and cationic, respectively. Next to each structure are written from top to bottom the C−O, O−Fe, and Fe−S bond distances, in Å.

***Table 1.*** Relative Energies (in kcal mol$^{-1}$) of a Few Transition State (TS) Species in the Gas Phase, under the Influence of Two NH···S Hydrogen Bonds and in a Polarizing Environment[a]

| transition state | $\Delta E_{gas}$ | $\Delta E_{NH\cdots S}$ | $\Delta E_{\epsilon=5.7}$ | $\Delta E_{NH\cdots S,\epsilon=5.7}$ |
|---|---|---|---|---|
| $^4$**TS**$_{1,2}$ | +2.6 | +5.6 | +4.2 | +7.2 |
| $^2$**TS**$_{1,2}$ | −0.6 | +0.2 | +0.5 | +0.9 |
| $^2$**TS**$_{1,3}$ | 0.0 | 0.0 | 0.0 | 0.0 |

[a] All values were taken from the calculation with Jaguar 4.1. The dielectric constant $\epsilon$ is 5.7.

hydrogen bonding capability, as in the protein pocket, the ordering of $^2$**TS**$_{1,2}$ and $^2$**TS**$_{1,3}$ is reversed; now $^2$**TS**$_{1,3}$ is 0.94 kcal mol$^{-1}$ lower than $^2$**TS**$_{1,2}$. The high-spin $^4$**TS**$_{1,2}$ undergoes the least stabilization by the environmental effects, and its energy rises to 7.2 kcal mol$^{-1}$ above the two low-spin TSs. This implies, in turn, that *the high-spin pathway will play a minor role in the reactivity of the enzyme and that the low-spin pathways will dominate*.

**B.3. Electronic Structure and Properties of the Reaction Intermediates.** To ascertain the nature of the $\sigma$-complexes ($^{4,2}$**2** and $^2$**3**), we characterized their electronic structures by use of natural orbital analyses. Figure 3 shows the main features of the lower lying $^2$**2** versus $^2$**3** intermediates, using the d-block and phenyl orbitals, group charges ($Q$), and group spin densities ($\rho$). It is seen that the $\sigma$-complex $^2$**2** is characterized by a d$^4$ configuration on iron, that is, Fe$^{IV}$, which is antiferromagnetically coupled to a single electron on the activated benzene moiety, in the $\phi_{Ph}$ orbital. The latter orbital is a nonbonding orbital of a pentadienyl moiety, in line with the formation of such a radical on the activated phenyl. This is further corroborated by the spin densities ($\rho$) on the iron and phenyl moieties, which are, respectively, 1.84 and −0.85.

In turn, in the $\sigma$-complex $^2$**3**, the nonbonding pentadienyl orbital is vacant, while the heme is characterized by a d$^5$ Fe$^{III}$ configuration. Thus, in fact, the complex $^2$**3** is *an internal ion pair*, obtained by transferring a single electron from the nonbonding orbital of the pentadienyl radical moiety, $\phi_{Ph}$, in $^2$**2**, to the singly occupied $\pi^*_{xz}$ orbital that becomes doubly occupied in $^2$**3**. We verified that the alternative cation $^2$**3**$_{yz}$ that arises by transferring the electron to the $\pi^*_{yz}$ orbital is much higher lying (7.28 kcal mol$^{-1}$, Table S.11). The singly occupied $\pi^*_{yz}$ orbital of $^2$**3**, in Figure 3, has a high d$_{yz}$(Fe) character, but it is also significantly delocalized over the phenyl moiety, and this is the origin of the spin density on the phenyl moiety. Note however that, in accord with its assignment, the carbocationic $\sigma$-complex $^2$**3** has a smaller phenyl spin density, $\rho$(Ph), and larger phenyl positive charge, $Q$(Ph), compared with those of the radicalar species, $^2$**2**. This is further corroborated by the effect of NH···S hydrogen bonding and medium polarity on these quantities, as may be witnessed by the corresponding values in parentheses. Thus, now the spin density on the phenyl moiety of $^2$**3** becomes quite small and negative, while the positive charge increases (to +0.68). In addition, the relative energy data reveals that the environmental effect stabilizes, $^2$**3**, well below the radical one, by ca. 4.6 kcal mol$^{-1}$. These effects are in line with the ion pair nature of $^2$**3** by contrast to the largely radicalar nature of $^2$**2**.

**B.4. Ring Closure Step.** The ring closure step, en route to the epoxide complex ($^2$**4**), in Figure 2 involves three TSs, two for the radicalar intermediates, $^{4,2}$**2**, and one for the cationic $\sigma$-complex intermediate, $^2$**3**. As in all previous studies,[21,22] here too, the low-spin radicalar process, via $^2$**TS**$_{2,4}$, has a lower barrier than the corresponding high-spin process, via $^4$**TS**$_{2,4}$. This will further diminish the contribution of the high-spin process in this reaction. The different nature of the intermediate $^2$**2** viz. $^2$**3** is reflected in fact in the relative ring closure barriers. Thus, the cationic $\sigma$-complex, which involves a cation−anion com-

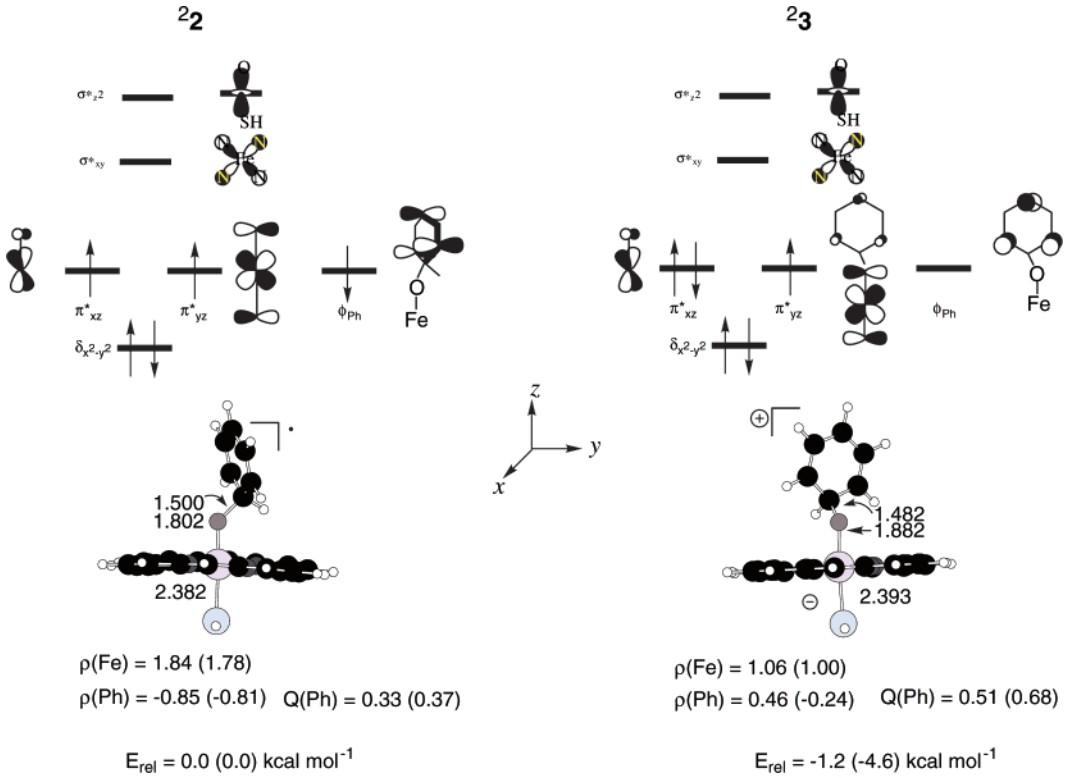


***Figure 3.*** Orbital occupancy, bond lengths (in Å), group spin ($\rho$) densities, charge densities ($Q$), and relative energies (kcal mol$^{-1}$) of the radicalar ($^2$**2**) and cationic ($^2$**3**) $\sigma$-complex intermediates. Only d-block orbitals ($\delta$, $\pi^*_{FeO}$, and $\sigma^*$) and the singly occupied or vacant benzene orbital ($\phi_{Ph}$) are shown. The relative energies are shown in the gas phase (out of parentheses) and with inclusion of NH···S hydrogen bonds and polarization by a medium with a dielectric constant of $\epsilon = 5.7$. Note the increased stability of $^2$**3** by the polarity and hydrogen bonding effects.

***Table 2.*** Relative Barriers, in kcal mol$^{-1}$, for Ring Closures to Benzene Oxide ($^2$**4**) from the $\sigma$-Complex Intermediates, in the Gas Phase, under the Influence of Two NH···S Hydrogen Bonds and a Polarized Environment in Combination With Two NH···S Hydrogen Bonds[a]

| process | $\Delta E^{\ddagger}_{gas}$ | $\Delta E^{\ddagger}_{NH\cdots S}$ | $\Delta E^{\ddagger}_{NH\cdots S,\epsilon=5.7}$ |
|---|---|---|---|
| $^2$**(2→ 4)** | 4.3 | 6.3 | 4.1 |
| $^2$**(3→ 4)** | 0.8 | 0.3 | 0.8 |

[a] All data were taken from Jaguar 4.1. The dielectric constant $\epsilon$ is 5.7.

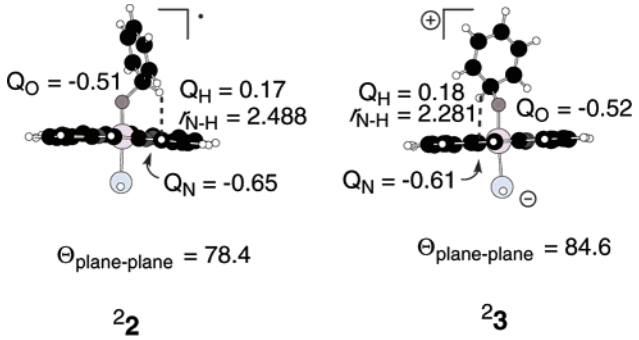


***Figure 4.*** Properties of the doublet $\sigma$-complex intermediates. Shown are group charges ($Q$), the N···H distance, and the phenyl plane−porphyrin plane angle ($\Theta_{plane-plane}$).

bination, has a tiny barrier of 1.2 kcal mol$^{-1}$, while the radical $\sigma$-complex has a significant barrier, ca. 3.3 kcal mol$^{-1}$. This reflects both strain and loss of delocalization energy of the pentadienyl radical in the radical intermediates. *Furthermore, given the energy difference of 4.6 kcal mol$^{-1}$ under environmental effects between $^2$**3** and $^2$**2** (Figure 3), their equilibration will not be very fast and is unlikely to yield much of the radicalar species*. As such, the cationic mechanism will dominate arene oxide production, while the radicalar mechanisms will be a minor pathway. Environmental effects on the barriers for ring closure of the two doublet processes are summarized in Table 2. The NH···S hydrogen bonding and the medium polarity have hardly any effect on these barriers.

**C. Mechanisms of Phenol and Ketone Production.** To test whether benzene oxide is the precursor of phenol or the ketone, we ran extensive geometry scans (see Figures S.5 and S.7, Supporting Information) following the transfer of the hydrogen atom from the tetrahedral carbon atom in $^{4,2}$**4** to the oxygen or to the *ortho* carbon of the phenyl group. All these scans led to high-energy pathways, which do not yield the desired end products. Thus, under the vacuum conditions employed in the calculations, the arene oxide complex ($^{4,2}$**4**) is not an intermediate in the formation of either phenol or ketone but a dead-end product. Nevertheless, as shown by Jerina and Daly,[4] arene oxides undergo rearrangement to phenols under physiological conditions and even exhibit NIH shift. Indeed, our calculations cannot account for such a rearrangement, which may transpire via protonation of the arene oxide, by a sequestered hydronium ion or an array of water molecules held by a side chain amino acid.[39] The question we wish to answer is *whether there can be a direct enzymatic pathway for the generation of phenol and ketone, not via the benzene oxide*.

It is apparent that an enzymatic NIH shift must involve an internal acid−base process. Initial appreciation of such a

(39) For sources of protonation and mechanisms thereof inside the protein, see: (a) Yeom, H.; Sligar, S. G.; Li, H.; Poulos, T. L.; Fulco, A. J. *Biochemistry* **1995**, *34*, 14733−14740. (b) Vidakovic, M.; Sligar, S. G.; Li, H.; Poulos, T. L. *Biochemistry* **1998**, *37*, 9211−9219. (c) Loew, G. H.; Harris, D. L. *Chem. Rev.* **2000**, *20*, 407. (d) Gualar, V.; Harris, D. L.; Batista, V. S.; Miller, W. H. *J. Am. Chem. Soc.* **2002**, *124*, 1430−1437.

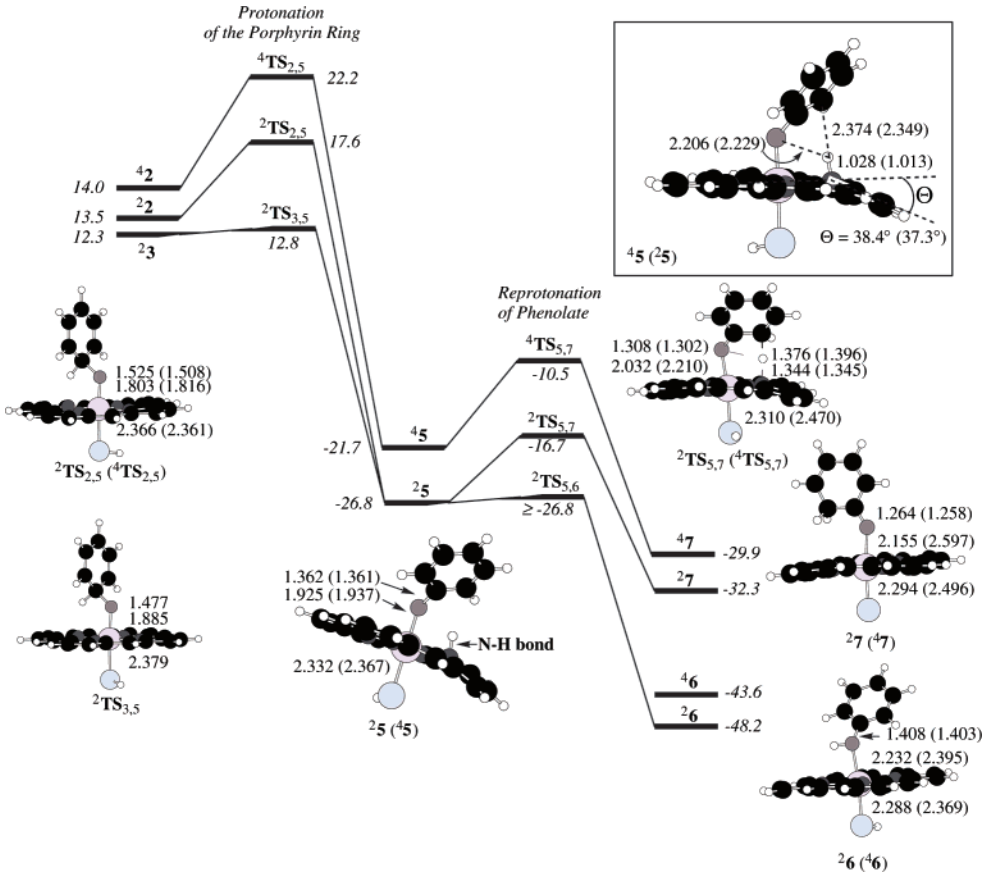


***Figure 5.*** Lowest doublet and quartet spin potential energy profiles for the formation of phenol and ketone from the $\sigma$-complex intermediates by proton shuttles. All values are in kcal mol$^{-1}$ relative to the reactants (in Figure 1). The conversions $^2$**3** to $^2$**5** and $^{4,2}$**5** to $^{4,2}$**6** involve flat energy profiles, and TSs could not be precised. Next to each structure are written from top to bottom the C−O, O−Fe, and Fe−S bond distances, in Å.

potential mechanism can be gained by inspecting the geometry of the intermediates, $^2$**2** and $^2$**3**, which are plotted again with additional details in Figure 4. As may be seen, the plane of the benzene ring is perpendicular to the porphyrin plane and neither parallel nor halfway between, as reported previously.[10] In the perpendicular orientation, the intermediates can be stabilized due to orbital mixing between the $\pi^*_{FeO}$ orbital of the iron−oxo moiety and the $\pi$ and $\pi^*$ orbitals of the benzene moiety. This interaction is less efficient when the benzene ring is parallel to the porphyrin plane. An additional important factor that stabilizes the perpendicular conformation relative to the parallel one is the interaction between the positively charged *ipso* hydrogen ($Q_H$(**2**) = 0.17, $Q_H$(**3**) = 0.18) of benzene and the negatively charged nitrogen atoms ($Q_N$(Por, **2**) = −0.65, $Q_N$(Por, **3**) = −0.61) of the porphyrin ring. As will turn out, it is this N···H(*ipso*) interaction that is crucial in the enzymatic conversion mechanism of the $\sigma$-complexes to the phenol and ketone products.

Figure 5 shows the energy profiles, which convert the $\sigma$-complex intermediates to the phenol (**6**) and ketone (**7**) products; for completeness, we show also the quartet state processes. As can be seen, starting from either $^{4,2}$**2** or $^2$**3**, one of the nitrogen atoms of the porphyrin ring abstracts the *ipso* hydrogen from the tetrahedral carbon of the $\sigma$-complex producing the protonated porphyrin complex ($^{4,2}$**5**). In the case of the radicalar $\sigma$-complexes, the abstraction is accompanied by shifting the radical from the benzene moiety to the $\pi^*_{xz}$ orbital of the heme (Figure 3), such that the process involves electron plus proton shifts. In the case of the cationic $\sigma$-complex, the abstraction is a simple proton-transfer process. As such, the process $^2$**3** → $^2$**5** has a small barrier that could not be localized precisely due to the extreme flatness of the surface. By contrast, the processes $^2$**2** → $^2$**5** and $^4$**2** → $^4$**5** have substantial barriers of 4.1 and 8.2 kcal mol$^{-1}$, respectively. The structure of the protonated porphyrin intermediate, $^{4,2}$**5**, is drawn in the inset in Figure 5. It is seen that the protonation causes a severe buckling of the porphyrin, such that one of the pyrrole rings deviates from the mean plane of the rest of the porphyrin by as much as 37−38°. A similar buckling was observed by us[21c] for the heme-alkylated product during the deactivation of the enzyme, en route to ethene epoxidation. This buckling appears also in the crystal structures of *N*-alkylporphyrins and *N*-alkylmetalloporphyrins.[40]

Another interesting feature of $^{4,2}$**5** is the proximity of the hydrogen end of the N−H bond to the oxygen and *ortho* carbon atoms of the phenoxyl moiety. As such, the protonated porphyrin species, $^{4,2}$**5**, can shuttle the hydrogen back to the substrate moiety. A proton shuttle to the oxygen atom produces phenol ($^{4,2}$**6**), while a shuttle to the *ortho* position of benzene produces 2,4-cyclohexenone ($^{4,2}$**7**). Since the oxygen position in $^{4,2}$**5** is negatively charged ($Q_O$ = −0.62 in $^2$**5**), much more so than the *ortho* carbon ($Q_C$ = −0.18 in $^2$**5**), production of phenol, $^{4,2}$**5** → $^{4,2}$**6**, meets only a tiny barrier, which could not be precised due to the flat surface. By contrast, production of the ketone, $^{4,2}$**5** → $^{4,2}$**7**, requires significant barriers of 10.2 (doublet) and 11.2 (quartet) kcal mol$^{-1}$. Nevertheless, since $^{4,2}$**5** and its subsequent species all lie well below the bond activation transition states

(40) For example, see: Lee, H.-I.; Dexter, A. F.; Fann, Y.-C.; Lakner, F. J.; Hager, L. P.; Hoffman, B. M. *J. Am. Chem. Soc.* **1997**, *119*, 4059−4069.

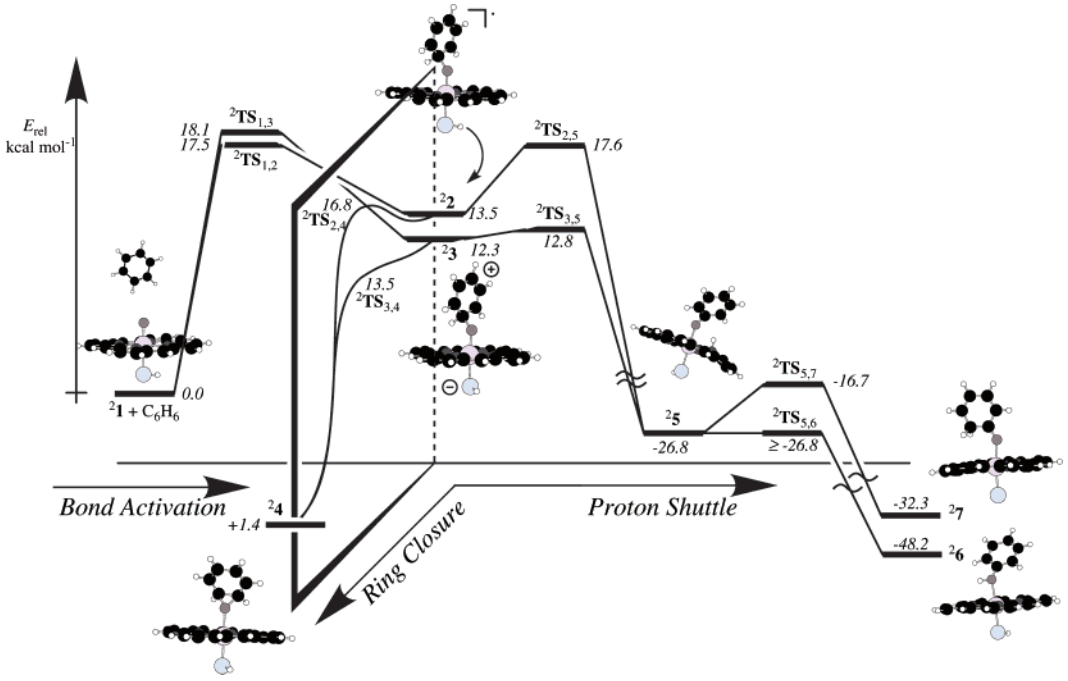


***Figure 6.*** Mechanistic scheme for the oxidation of benzene to benzene oxide, phenol, and ketone. Only the doublet low-spin mechanisms are shown. Relative energies are in kcal mol$^{-1}$ relative to the reactants. Note that NH···S hydrogen bonding and medium polarity lower $^2$**TS**$_{1,3}$ ca. 1 kcal mol$^{-1}$ below $^2$**TS**$_{1,2}$ and $^2$**3** 4.6 kcal mol$^{-1}$ below $^2$**2** (see Table 1).

in Figure 1 ($^2$**TS**$_{1,3}$), then, in the case that $^2$**5** does not undergo fast thermalization within the protein pocket, there will exist sufficient excess energy to pass the barrier for rearrangement of $^2$**5** to cyclohexenone. The assumption that $^2$**5** is not thermalized requires that some of the excess energy, ca. 10 kcal mol$^{-1}$, will not dissipate to the protein but will be invested in the internal modes of $^2$**5**, thereby serving to drive $^2$**5** to $^2$**7**. It follows that, since the conversion of the intermediate to phenol is almost barrierless, this process will compete efficiently with any post-enzymatic conversion of the benzene oxide to phenol via protonation by an external source (e.g., sequestered hydronium ion, amino acid side chain, etc[39]). Moreover, under the assumption of an incomplete thermalization of $^2$**5**, its rearrangement to cyclohexenone will also be competitive with a post-enzymatic rearrangement of benzene oxide that requires initial dissociation from the heme complex.

To ascertain whether $^2$**2** and $^2$**3** could rearrange to phenol and ketone by other pathways that may account for the NIH shift, we tested 1,2-hydrogen shifts from the *ipso* carbon either to the oxygen or to the *ortho*-carbon. As may be seen from the Supporting Information (Figures S.8 and S.9) starting from the radical intermediate $^2$**2**, the energy rises very steeply, while in the case of $^2$**3** the scan simply falls to the protonated heme intermediate, $^2$**5**. Another potential pathway that was studied is the 1,3-hydrogen shift in $^2$**2** and $^2$**3**. In this process too, starting from $^2$**2**, the energy rises very steeply (Figure S.12), while when starting from $^2$**3**, the scan simply falls to the protonated heme intermediate, $^2$**5**. Attempts to prevent $^2$**3** from undergoing instantaneous heme protonation, by angular constraints, resulted in a very steep energy rise en route to the 1,3-shifted species (Figure S.12). Apparently, *the coordinated carbocation in the internal ion pair species* $^2$***3*** *does not behave like a free carbocation* and does not undergo facile hydrogen shifts, most likely because it is engaged in bonding with the iron−oxo moiety. Thus, one could be reasonably confident that the major mechanism for the production of phenol and ketone *within the coordination sphere of iron* proceeds via the intermediary of $^2$**5**. Of course, we cannot rule out tunneling from $^2$**2** and $^2$**3** to phenol and ketone, but if tunneling is important, it will also operate in the conversions of $^2$**2** and $^2$**3** to the requisite products via $^2$**5**.

## Discussion

**A. Differences and Similarities between the Mechanistic Schemes of Benzene Oxidation and Olefin Epoxidation by Cpd I.** Figure 6 assembles the lowest energy mechanisms, from Figures 2 and 5, into a single mechanistic scheme. The viable mechanisms proceed via low-spin (LS) radicalar and carbocationic pathways, and the corresponding $\sigma$-complex intermediates, $^2$**2** and $^2$**3**, branch out to all the products ($^2$**4**, $^2$**6**, and $^2$**7**). The levels of the high-spin (HS) species are not shown, since the HS transition states (TSs) are much higher in energy and become even higher by medium polarity and hydrogen bonding interactions with the thiolate ligand (Table 1). In this sense, benzene oxidation is fundamentally different than other mechanisms which were studied so far, namely C−H hydroxylation[23c,d,25] and C═C epoxidation[21,22] by Cpd I. All other mechanisms were found to involve two-state reactivity[41,42] in terms of the interplay of HS and LS radicalar pathways and occasionally also species that differed in the oxidation state of the iron ($Fe^{III}$ and $Fe^{IV}$). By contrast, *benzene oxidation, to whichever product, is dominated by the LS pathways, where now it is the substrate that appears in different "oxidation states", one radicalar and one cationic*. This difference merits elaboration.

As noted already, there seems to be a fundamental reason why the HS bond activation transition state ($^4$**TS**$_{1,2}$) is signifi-

(41) Schröder, D.; Shaik, S.; Schwarz, H. *Acc. Chem. Res.* **2000**, *33*, 139−145.
(42) Shaik, S.; de Visser, S. P.; Ogliaro, F.; Schwarz, H.; Schröder, D. *Curr. Opin. Chem. Biol.* **2002**, *6*, 556−567.

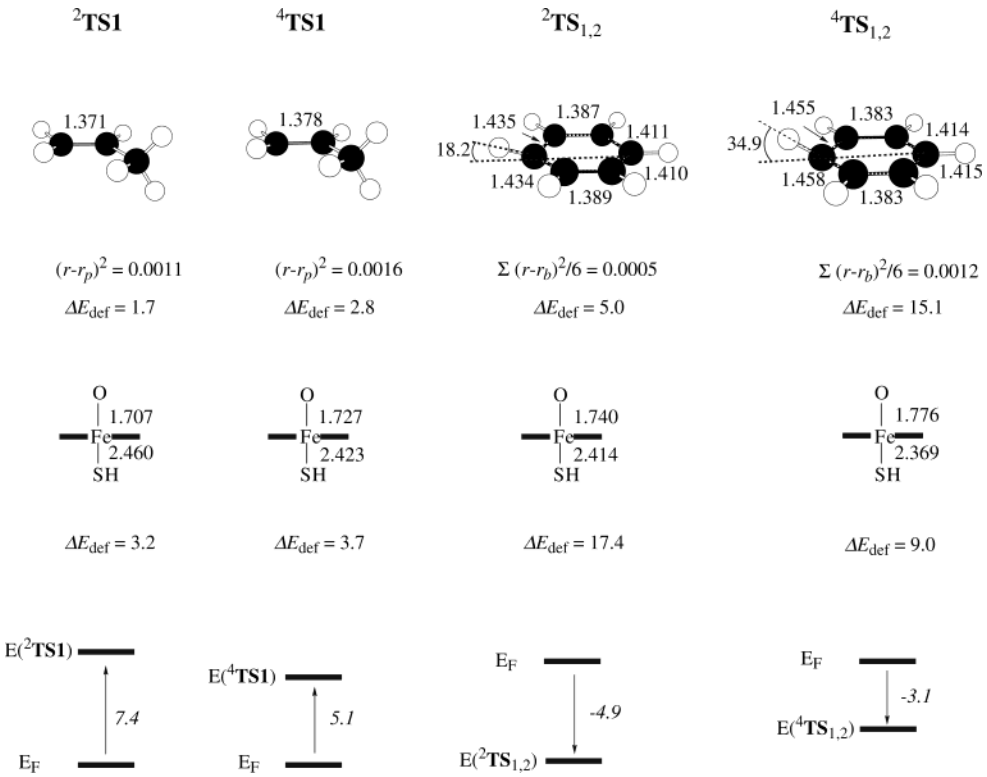


***Figure 7.*** Structural distortions and deformation energies (in kcal mol$^{-1}$) in the high-spin (HS) and low-spin (LS) transition states ($^4$**TS**$_{1,2}$ viz. $^2$**TS**$_{1,2}$) for benzene oxidation viz. propene epoxidation. The bond distortion is indexed as averaged squared deviations relative to the free substrate. The pyramidalization angles are shown explicitely. The relative deformation energies are given as $\Delta E_{def}$. The total fragment energies ($E_F$) are shown relative to the energy of the transition states ($E$(**TS**)). Note the difference between the propene and benzene reactions.

cantly higher than its LS counterpart. This is analyzed in Figure 7, by comparing the structural deformations of the moieties in the HS and LS TSs, the corresponding deformation energies for substrate activation, and the energies of the deformed moieties ($E_F$) relative to the respective TSs ($E$(**TS**)), in the case of propene[22] viz. benzene. As shown by the bond length deviation index and the angular distortions relative to the free substrate, in both processes, the HS species, $^4$**TS**, involves a higher degree of substrate deformation compared with its LS counterpart, $^2$**TS**. However, other than that, the deformation patterns are drastically different for the two processes. In the case of propene, the substrate deformation energy is higher by merely 1.1 kcal mol$^{-1}$ in $^4$**TS1**, relative to $^2$**TS1**, and the Cpd I moiety undergoes equally small deformations. Indeed, the sum of the deformation energies of the TS constituents is well below the barrier by 5.1−7.4 kcal mol$^{-1}$, whereas the barrier itself is ca. 10 kcal mol$^{-1}$. Thus, the TSs for propene epoxidation are an "early" species that resemble the ground-state species. As such, the TSs exhibit close lying HS and LS species,[21,22] much as in the ground state, where these states nascent from Cpd I are close lying.

By contrast, in the case of benzene, the substrate activation is accompanied by a loss of resonance energy and would require a large deformation of the molecule. As may be seen in Figure 7, the benzene molecule is significantly distorted (consider the angular deformation and bond deformation index), and the deformation energies are much larger than in propene. Importantly, the $\Delta E_{def}$ quantity of the HS species ($^4$**TS**$_{1,2}$) is now 10.1 kcal mol$^{-1}$ larger compared with the LS counterpart ($^2$**TS**$_{1,2}$). *These large deformation energies reflect that, in its ground state, benzene is stabilized by resonance energy and requires therefore significant deformation in order to be activated*. Indeed, the Cpd I moiety, in these TSs, undergoes also large deviations from its ground-state geometry. Consequently, the sum of deformation energies of the TS fragments is higher than the corresponding barriers by 3.1−4.9 kcal mol$^{-1}$. These latter quantities constitute the total interaction energies of the TS fragments to yield the final states, $^2$**TS**$_{1,2}$ and $^4$**TS**$_{1,2}$. Thus, the TSs for benzene hydroxylation are a very "late" species that do not resemble anymore their ground states. As such, the HS−LS energy difference will no longer be small, as in the ground state, and will be dominated by other factors. Our energy partition, in Figure 7, shows that the difference of 3.1 kcal mol$^{-1}$ in the barriers originates in a combination of (i) a higher deformation energy of the benzene moiety in the $^4$**TS**$_{1,2}$ species and (ii) the poorer binding between the benzene moiety and the iron−oxo species in the $^4$**TS**$_{1,2}$ species. Polarity and NH···S hydrogen bonding further increase this difference to 6.3 kcal mol$^{-1}$ (Table 1). The very same trend is exhibited for the TS species ($^{2,4}$**TS**$_{1,3}$) of the cationic pathway, where the deformation energy of the $^4$**TS**$_{1,3}$ species is higher by 4 kcal mol$^{-1}$ compared with the LS counterpart. These large differences in the substrate deformation energies raise the HS TS species considerably above the corresponding LS species. It follows therefore that the LS mechanism will dominate arene oxidation due to a fundamental property of arenes, their $\pi$-delocalization, that enforces large deformations in the TS. Small, residual HS reactivity may transpire primarily by spin crossover between the HS and LS radicalar $\sigma$-complexes (e.g., $^{2,4}$**2** in Figure 2), a process that may be too inefficient to matter.

Another major difference between olefin epoxidation and benzene hydroxylation, is the appearance of the cationic pathway

in the case of benzene, by contrast to the radicalar-only pathways that operate in the case of olefins.[21,22] The reason for this difference can be understood by considering the conversion of the radicalar $\sigma$-complex to the cationic one, for example, $^2$**2** → $^2$**3** in the present problem, via internal electron transfer from the radical moiety to the heme. The relative facility of the process for different substrates will depend on the ionization energy of the substrate-derived radical. In the case of benzene, the radical $\sigma$-complex, $^2$**2**, involves a *cis*-pentadienyl radical moiety, derived from the benzene, linked to the heme, while, in propene activation, the analogous $\sigma$-complex involves an alkyl (ethyl-like or isopropyl-like) radical. Since the ionization potential of the *cis*-pentadienyl radical is lower than that of the alkyl radical by as much as 13−30 kcal mol$^{-1}$,[43] the cationic $\sigma$-complex could be located by us only during benzene oxidation. However, it is apparent that when the olefin-derived radical moiety will become a better electron donor, then cationic $\sigma$-complexes will be significant also during olefin epoxidation, as we already reasoned before.[21a] Thus, in accord with the mechanisms deduced from experiment, the mechanistic schemes of arene hydroxylation and olefin epoxidation can indeed be unified,[11,18] with the addition of the two-state reactivity aspect of olefin epoxidation that emerges from theory.[21,22]

An aspect worth mentioning at this point is associated with the feasibility of the electron-transfer process. As can be seen from Figure 1, the separated electron transferred intermediates lie ca. 120 kcal mol$^{-1}$ above the cationic $\sigma$-complex. In fact, the latter intermediate is a result of the bonding of the two electron transferred species. This bonding energy is composed of the electrostatic interactions and the C···OFe bond energy; its magnitude is sufficiently large to severely limit the concentration of a diffusive radical cation of the substrate even for polycyclic aromatic species.

**A.1. Reactivity Patterns viz. Other P450 Processes.** Figure 6 reveals that the benzene activation via $\pi$-attack is the rate-determining step for all the mechanisms. It is therefore instructive to assess the reliability of the computed scheme by comparison to other computations and to experimental trends. In a vacuum, the lowest barrier in Figure 6, 17.5 kcal mol$^{-1}$, is via $^2$**TS**$_{1,2}$ that leads to the radical $\sigma$-complex ($^2$**2**). The competing process via $^2$**TS**$_{1,3}$ that leads to the carbocationic $\sigma$-complex ($^2$**3**) has a slightly higher barrier, 18.1 kcal mol$^{-1}$. With inclusion of the environmental effects that simulate the protein polarity and hydrogen bonding capability, the order of the transition states is reversed and the cationic mechanism has the lowest barrier (Table 1). In any event, the barrier for the rate-determining step is of the order of 16.5−18.1 kcal mol$^{-1}$. These barriers are significantly higher than the computed barriers for the epoxidation of propene,[22] which are 10.3 (HS) and 10.6 (LS) kcal mol$^{-1}$ and also higher than those for ethene epoxidation,[21] which are 13.9 (HS) and 14.9 (LS) kcal mol$^{-1}$. Thus, the computations predict that olefin epoxidation should be energetically favorable over phenyl epoxidation/hydroxylation. Indeed, experimentally the oxidation of, for example, styrene by Cpd I leads to epoxidation of the vinyl group with only a trace of phenyl hydroxylation.[1,18−20] Similarly, the allylic hydroxylation of propene was computed to have barriers of 10.6 (HS) and 10.8 (LS) kcal mol$^{-1}$,[22] which are significantly lower than the presently calculated barriers for benzene hydroxylation/epoxidation. Again, this is in good agreement with the experimental observation of toluene oxidation, which gives predominantly benzyl alcohol via benzylic C−H hydroxylation, with little if ever phenol production.[44] By contrast, C−H hydroxylation in simple alkanes was computed to have larger barriers of 19−27 kcal mol$^{-1}$, depending on the alkane.[23,45] As already reasoned before[18,19,22,23c] C−H hydroxylation is very sensitive to the C−H bond strength. Therefore, one may reasonably expect that by using the Newcomb probes, such as *trans*-2-methylphenylcyclopropane, C−H hydroxylation will be faster than in simple alkanes and compete with phenyl epoxidation. Indeed, as shown by Newcomb et al.,[46] phenyl hydroxylation becomes appreciable only after deuteration of the methyl group of *trans*-2-methylphenylcyclopropane, which results in metabolic switching and produces more of the phenol product. Thus, the computational results in this paper together with previous studies form a reliable set of data that matches experimental trends.

**B. Benzene Epoxidation viz. Hydroxylation: Are They Connected?** As discussed in the Introduction, the major dilemmas in the field of arene oxidation concerns the precise role of the radicalar viz. the cationic $\sigma$-complexes in the mechanism, the obligatory intermediacy of arene oxide en route to phenol and ketone, and the origins of the NIH shift (Scheme 1). Figure 6 allows us to respond to these questions and help resolve the mechanistic puzzle.

**B.1. Competition between the Radicalar and Cationic Mechanisms of Benzene Activation.** It is apparent from Figure 6 that two factors determine the relative importance of the two pathways, the relative barriers of bond activation via $^2$**TS**$_{1,2}$ viz. $^2$**TS**$_{1,3}$ and the partition of the intermediates $^2$**2** viz. $^2$**3** to the various products. First, under conditions that mimic the electrostatic and hydrogen bonding interaction in the protein pocket, the lowest species is $^2$**TS**$_{1,3}$ (2NH···S, $\epsilon = 5.7$) that leads to the cationic intermediate (Table 1). Second, the barrier for collapse of the cationic $\sigma$-complex, $^2$**3**, to give either the benzene oxide ($^2$**4**) and/or the protonated heme intermediate ($^2$**5**), is significantly smaller than the corresponding barriers nascent from the radical $\sigma$-complex, $^2$**2**. Finally, with hydrogen bonding and polarity effect included, $^2$**3** becomes much lower than the radicalar intermediate by 4.6 kcal mol$^{-1}$. Consequently, the cationic mechanism will prevail, and one may estimate, from the relative bond activation barriers, that an upper limit contribution of the radicalar mechanism to arene oxide formation will be approximately 17% at $T = 300$ K.

**B.2. Phenol and Ketone Production: Must They Originate from Benzene Oxide?** As we showed in the Results section, in vacuum, there is no pathway that rearranges the iron−oxo coordinated $\sigma$-complex intermediates to either phenol or ketone. These intermediates branch out to give either the new intermediate $^2$**5** and/or benzene oxide. Furthermore, in vacuum, there is no pathway that converts benzene oxide directly to phenol and ketone. In this respect, the calculations in a vacuum suggest that benzene oxide is a dead-end product. However, arene oxides

(43) Ionization potentials were computed with the OVGF method described in: Danovich, D.; Apeloig, Y.; Shaik, S. *J. Chem. Soc., Perkin Trans. 2*, **1993**, 321.

(44) (a) Inchley, P.; Lindsay-Smith, J. R.; Lower, R. J. *New J. Chem.* **1989**, *13*, 669−676. (b) Baciocchi, E.; Crescenzi, M.; Lanzalunga, O. *Chem. Commun.* **1990**, 687−688.

(45) Cohen, S.; Shaik, S., unpublished results for gas-phase hydroxylation of camphor.

(46) (a) Newcomb, M.; Toy, P. H. *Acc. Chem. Res.* **2000**, *33*, 449−455. (b) Newcomb, M.; Shen, R.; Choi, S.-Y.; Toy, P. H.; Hollenberg, P. F.; Vaz, A. D. N.; Coon, M. J. *J. Am. Chem. Soc.* **2000**, *122*, 2677−2686.

are known[4] to give phenols when in appropriate media that can protonate the epoxide or catalyze its ring opening. Thus, our calculations cannot, of course, rule out that part of the phenol product arises from a pathway that involves external protonation of the arene enzyme under physiological conditions.[39] However, our computations propose *an enzymatic alternative*, which is the proton-shuttle mechanism, shown in Figure 6 (also Figure 5). In this mechanism, the nitrogen atoms of the porphyrin act as internal bases and abstract a proton from the $\sigma$-complex intermediates, $^2$**3** and $^2$**2**, to yield the protonated porphyrin intermediate, $^2$**5**. This intermediate subsequently transfers the proton back either to the oxygen to produce phenol, $^2$**6**, or to the *ortho* carbon to produce the ketone, $^2$**7**. *The barrier* $^2$**5** → $^2$**6** *is exceedingly small, and one can be assured that this proton-shuttle mechanism will be competitive with the externally assisted ring opening of the benzene oxide (e.g., by external acid catalysis)*. Furthermore, since the transition state $^2$**TS**$_{5,7}$ lies well below the $\sigma$-complex intermediate $^2$**3**, then, in the case of incomplete thermalization of $^2$**5**, part of this great excess energy will serve to drive the conversion of $^2$**5** to $^2$**7**. This process, which is largely controlled by energy transfer among the internal modes of the molecule, may also compete with the acid-catalyzed benzene oxide conversion to $^2$**7**. Another way to conceptualize the role of the proton-shuttle mechanism is that it serves as a catalytic process whereby the enzyme generates phenols from arenes directly. Thus, as we showed earlier in Figure 1, the rebound mechanism for phenol formation requires a barrier that is too high, by at least 10 kcal mol$^{-1}$ (see also Figure S.10), compared with the present mechanism. *Clearly, the enzyme bypasses all the high-energy processes and utilizes the porphyrin ligand as a springboard for mediating phenol production (and in part also the ketone) from arene.*

An assessment of the benzene oxide viz. phenol (and ketone) production can be made by considering, in the light of Figure 6, the partitioning of $^2$**3** and $^2$**2** to the arene oxide $^2$**4** viz. the protonated porphyrin intermediate $^2$**5**. It is seen that the barriers for the processes $^2$**3** → $^2$**4** viz. $^2$**3** → $^2$**5** are roughly of the same order, and so are the barriers for $^2$**2** → $^2$**4** viz. $^2$**2** → $^2$**5** (Figure 2). It follows therefore that benzene oxide production will be competitive with phenol production. Of course, in our vacuum calculations, the two products are orthogonal and do not interconnect, whereas, under physiological conditions, much of the arene oxide may convert to phenolic products, either by direct opening or by reacting with various cellular nucleophiles (DNA, the protein, sequestered water, etc).

Scheme 2 summarizes the computationally derived mechanism using deuterated benzene to illustrate the NIH shift. Thus, our calculations reveal that the cationic $\sigma$-complex, $^2$**3**, plays the major role in producing all the products, while the radical, $^2$**2**, plays a relatively minor role. Moreover, in agreement with Korzekwa et al.[6] and Rietjens et al.,[7] the calculations show that arene oxide *is not the only* precursor of phenol and ketone. Our scheme predicts that, in addition, as part of the direct enzymatic reaction, there exists an internal proton-shuttle mechanism that accounts for the production of phenol as well as for NIH shift.[1,2,4]

This unusual mechanism could well be general, and protonated porphyrin intermediates may play a frequent mechanistic role in P450 chemistry. For example, such an intermediate may be responsible for the intriguing finding of Groves et al.,[18,27]

***Scheme 2.*** Computationally Based Mechanism of Benzene Oxidation by Cpd I.[a]

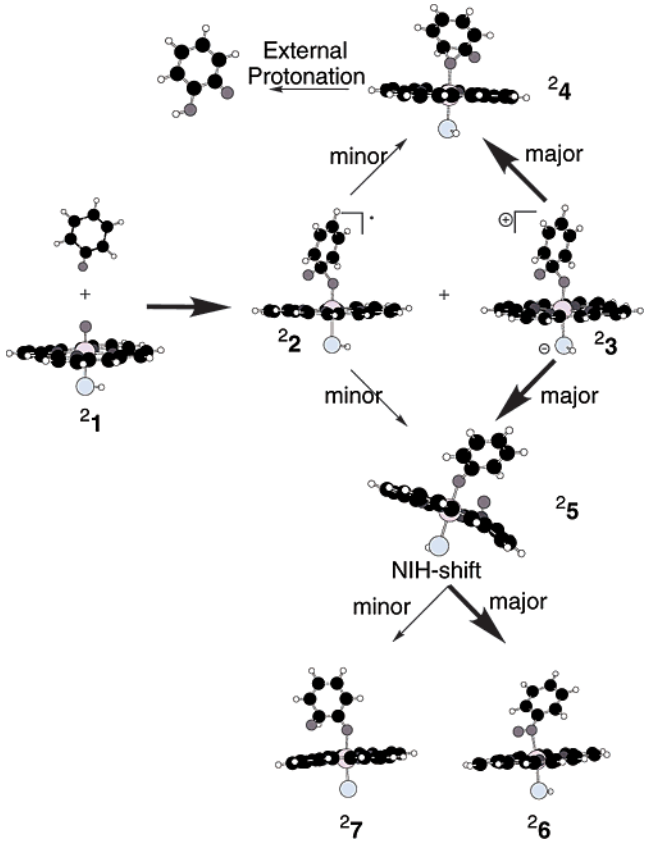


[a] Minor and major pathways are indicated. Note that the NIH shift occurs by the proton-shuttle mechanism via the protonated porphyrin intermediate ($^2$**5**). The possibility of opening of the benzene oxide to phenol by post-enzymatic processes (e.g., acid catalysis) is indicated too.

that epoxidation of propene and other terminal alkenes by P450$_{LM2}$, in the presence of $D_2O$, lead to an unusual hydrogen/deuterium exchange at the terminal position. A protonated porphyrin intermediate of the type $^2$**5** or $^4$**5** (but with an alkene instead of arene) having a finite lifetime will exchange protons with external acids including water. The protonated heme intermediate is reminiscent of the mechanisms of heme alkylation that occurs during the epoxidation of terminal olefins.[1,26] However, while heme alkylation destroys the catalyst, *the protonated intermediate catalyzes the C−H hydroxylation*. The protonated heme intermediate, $^2$**5**, and the heme alkylation complexes begin to map a gallery of porphyrin intermediates as well as their mechanistic origins and roles during oxidative processes by P450.

## Conclusions

The density functional calculations of benzene hydroxylation by a model Cpd I of Cytochrome P450 respond to the major dilemmas in the area[1,2] and project some novel features of the mechanisms. In harmony with experiment,[6,7] the theoretical calculations show that benzene activation occurs by an initial attack on the $\pi$-system of the benzene to produce $\sigma$-complexes along electrophilic and radicalar pathways. The dominant reaction channel is electrophilic leading to the cationic $\sigma$-complex, $^2$**3**, while the minor channel involves the intermediacy of the radical $\sigma$-complex, $^2$**2**. Ring closure in these intermediates produces the benzene oxide product ($^2$**4**).

Benzene oxide does not rearrange to phenol ($^2$**7**) or cyclohexenone ($^2$**6**) and requires acid catalysis. The computations reveal a novel mechanism, whereby the active species of the enzyme participates as an internal base and catalyzes directly the production of phenol and cyclohexenone. This enzymatic mechanism involves proton shuttles mediated by the porphyrin ring, through the *N*-protonated intermediate, $^2$**5**. The formation of the phenol via this proton-shuttle mechanism is predicted to be fast enough to compete with the post-enzymatic conversion of benzene oxide to phenol by external acid catalysis. *Thus, the computationally discovered porphyrin protonation mechanism suggests that there is an enzymatic pathway that converts benzene directly to phenol and ketone, in addition to the post-enzymatic production of these species by conversion of arene oxide to phenol and ketone.*

The potential generality of protonated porphyrin intermediates in P450 chemistry is discussed in the light of the H/D exchange observed during some olefin epoxidation reactions[27] and the general observation of heme alkylation products.[26] The competition, similarities, and differences between benzene oxidation viz. olefin epoxidation and alkanyl C−H hydroxylation are discussed, and the comparison with relevant experimental and computational data is favorable.

The dominance of low-spin reactivity in benzene hydroxylation is analyzed, and it is shown that the root cause for this trend is the loss of benzene resonance energy during the bond activation step. Thus, the benzene deformation that is much larger in the high-spin transition state disfavors the high-spin process. By contrast, in alkene epoxidation or alkane hydroxylation, the deformation of the substrate is similar in the high-spin and low-spin transition states, and consequently, these processes occur by two-state reactivity.[21,22,25,42] In this sense, it has not eluded us that this difference has implications on the reactivity patterns of the Newcomb probes that involve both benzene and alkane hydroxylation processes in the same substrate.[46]

**Acknowledgment.** The research is supported in part by the Israeli Science Foundation (ISF), The Ministry of Science, Sports and Art, and the German Israeli Foundation (GIF).

**Supporting Information Available:** Tables (16) with relative energies, absolute energies, group spin densities, and group charges of all optimized geometries in the gas phase and with environmental effects are available. In addition, 12 figures and 3 schemes with detailed geometries of the optimized structures, geometry scans, and alternative reaction paths are available. This material is available free of charge via the Internet at http://pubs.acs.org.

JA034142F